Comprehensive study of the magnetic phase transitions in Tb_3Co combining thermal, magnetic and neutron diffraction measurements

A. Herrero [a], A. Oleaga [a, *], A. F. Gubkin [b, c], M. D. Frontzek [d, e], A Salazar [a], N. V. Baranov [b, c]

[a] Departamento de Física Aplicada I, Escuela de Ingeniería de Bilbao, Universidad del País Vasco UPV/EHU, Plaza Torres Quevedo 1, 48013 Bilbao, Spain
[b] M.N. Miheev Institute of Metal Physics, Ural Branch of the Russian Academy of Sciences, 620108 Ekaterinburg, Russia
[c] Institute of Natural Sciences and Mathematics, Ural Federal University, 620083 Ekaterinburg, Russia
[d] Oak Ridge National Laboratory, Neutron Scattering Division, Oak Ridge, 37831, TN, USA
[e]Paul Scherrer Institut, Laboratory for Neutron Scattering and Imaging, CH-5232 Villigen, Switzerland

[*]Corresponding author: Departamento de Física Aplicada I, Escuela de Ingeniería de Bilbao, Universidad del País Vasco UPV/EHU, Plaza Torres Quevedo 1, 48013 Bilbao, Spain. Phone +34946014008. E-mail: alberto.oleaga@ehu.es

ABSTRACT

A comprehensive study of the magnetic phase transitions in Tb_3Co has been undertaken combining different techniques. Using single crystal neutron diffraction in the paramagnetic state a weak crystal structure distortion from the room temperature orthorhombic structure of the Fe_3C type described with the *Pnma* space group toward structure with lower symmetry has been observed with cooling below 100 K. At 81 K there is a second order phase transition to an antiferromagnetic incommensurate phase with the propagation vector $\boldsymbol{k}$ = (0.155, 0, 0). As derived from thermal diffusivity measurements, the critical exponents for this transition are very close to the 3D-Heisenberg universality class, proving that the magnetic interactions are short-range but with a deviation from perfect isotropy due to crystal field effects. At $T_2 \approx 70$ K there is another magnetic phase transition to a ferromagnetic state whose character is shown to be weakly first order. The low temperature magnetic state has a non-coplanar ferromagnetic structure with strong ferromagnetic components of Tb magnetic moments along the crystallographic ***c***-axis. The application of an external magnetic field B = 2 T along the

c crystallographic axis suppresses the incommensurate antiferromagnetic phase and gives rise to the ferromagnetic phase. The magnetic entropy peak change as well as the refrigerant capacity indicate that Tb_3Co is a competitive magnetocaloric material in this temperature range.

Keywords: Critical behavior; Tb_3Co; neutron diffraction; spin-ordering ; thermal diffusivity; magnetocaloric effect.

*Corresponding author; E-mail: alberto.oleaga@ehu.es

1. Introduction

Rare-earth based intermetallic materials are currently being the object of a wide research due to their potential technological applications based, first on their magnetocaloric properties (which make them suitable for cryocoolers which could replace the ones based on the classic gas expansion-compression cycles) and, second, on the presence of giant magnetoresistance [1, 2]. R_nT_m (*R* rare earth, *T* transition metal) is one of those big intermetallic families, whose magnetic properties heavily depend on the rare earth contents. If the ratio *n:m* is small, the transition metal ions can have a net moment regardless of the magnetic state of the rare earth sublattice, whereas there is a decrease in the magnetic moment of the transition metal ions when the *n:m* ratio increases, due to the filling of the 3d band on *T* atoms by outer-shell electrons of *R* atoms [3-5], with the particularity that, in the case of *T*=Co, its magnetic moment is lost for a ratio *n:m* bigger than three. Prior to any technological development, it is paramount to have an insight as complete as possible of the physical properties of the magnetic phase transitions involved, such as their character, the way the spins are ordered, the extent of the interaction (short or long range order), etc.

Several studies have already been undertaken for R_3Co with different *R* such as Gd [6-11], Ho [9, 12], Er [9, 11, 13-14], Dy [11, 15-19], and Tb [9, 11, 20-24]. In this particular work, we are focusing on Tb_3Co as it presents quite a complex behavior and there are several issues not studied or resolved yet. As reported, there are two magnetic phase transitions in Tb_3Co, a first one at about 82 K, from a paramagnetic (PM) to an antiferromagnetic (AFM) phase and a second one at a lower temperature, about 72 K, with a change to a complex noncoplanar ferromagnetic (FM) phase, with the spins ordering along the easy c-axis, but with an AFM ordering along the a- and b- axes [22-

24]. Concerning the crystal structure, this is Fe_3C type structure with the orthorhombic *Pnma* space group. The magnetic structure of Tb_3Co is not commensurate with the crystal one as, at the PM-AFM phase transition, magnetic reflections can be indexed with the propagation vector $\boldsymbol{k}$ (0.155, 0, 0). Magnetic intensity on these position can be detected below the AFM-FM transition until about 66 K. Interestingly, at lowest temperature the neutron diffraction patterns can only be explained by a mixture of $\boldsymbol{k}$ = (0,0,0) and (0.32, 0.32, 0) [22], which implies that at the magnetic AFM-FM transition (72 K) the magnetic phase is still incommensurate with $\boldsymbol{k}$ = (0.155, 0, 0) and that only at a lower temperature the propagation vector changes.

The character of the PM-AFM transition is considered as second order but, as the two magnetic transitions are so close, there has not been much effort to study the AFM phase in detail; in particular, no critical behavior study has been performed, which is a very sensitive tool to assess if the magnetic order parameter is 3-dimensional or has lower dimensionality, as well as the range of the magnetic interactions (either short or long). On the other hand, the AFM-FM transition is believed to have a first order character, but this is based on indirect evidences. In particular, this has been interpreted from the shape of the specific heat curves, but without showing any thermal hysteresis or having calculated a latent heat [25, 26]. Besides, as mentioned before, neutron diffraction data suggest that there is a superposition of two magnetic structures [22] which may contribute differently to the specific heat.

Another interesting feature in Tb_3Co is that Tb occupies two non-equivalent positions: 4c (site symmetry m) and 8d (site symmetry I). The low symmetry orthorhombic crystalline structure in which Tb atoms occupy these two nonequivalent sites leads to an increase of the crystal field effect, which have been held responsible for the complexity of the magnetic properties revealed so far [22].

Therefore, the purpose of this paper is to study in detail the character and properties of the phase transitions using high resolution techniques, as well as confirming the potentiality of Tb_3Co as a magnetocaloric material, extending its knowledge and settling several unresolved issues mentioned in this introduction.

2. Samples and Experimental Techniques

A few Tb_3Co polycrystalline ingots were synthesized by arc melting in a helium atmosphere using Tb and Co of 99.9% and 99.99% purity, respectively. The single crystal sample with dimensions of approximately $3 \times 3 \times 4$ mm^3 was grown by remelting of the

pellets at temperatures just above the peritectic point in a resistance furnace with a high temperature gradient. The back-reflection Laue method was used for the as-grown single crystal characterization and attestation. No extra reflections from other grains were detected. Absence of additional grains and good quality of the single crystal was confirmed on the neutron diffraction experiment as well. Then the single crystal sample was cut into the plane-parallel slabs which are parallel to the (010) crystallographic plane. Those surfaces had been well polished and additionally checked by the back Laue method. The thicknesses of the slabs was about 600 μm.

A high resolution *ac* photopyroelectric calorimeter in the back detection configuration has been used for the thermal measurements. Thermal diffusivity has been obtained as a function of temperature from room temperature down to 30 K, paying special attention to the region around the magnetic transitions. This technique is very well suited to study the critical behavior in phase transitions and has been successfully applied to solid and liquid crystals (magnetic as well as ferroelectric transitions), including other intermetallic materials [19, 27-35], as it combines very low temperature rates (down to 5-10 mK/min) with a high sensitivity. The details of the experimental setup, as well as of the theory explaining how to extract the thermal diffusivity from the photopyroelectric signal, can be found elsewhere [29, 36]. With this technique, thermal diffusivity is measured in a direction perpendicular to the surface, the crystallographic plane (010) in this case.

Magnetization (M) measurements have been carried out in a VSM (Vibrating Sample Magnetometer) by Cryogenic Limited under external applied magnetic fields H_a ranging from 0 to 80 kOe. For the magnetocaloric studies, isotherms have been collected over a range of 50-145 K with ΔT = 1 K between 50-100 K, ΔT = 2 K between 100-120 K and ΔT = 5 K between 120-145 K. The applied magnetic field H_a has been corrected for demagnetization effects and the internal field calculated using the relation $H_i=H_a-NM$, where M is the measured magnetization and N the demagnetization factor. This demagnetization factor has been obtained using the method described in references [37, 38], measuring the zero-field ac susceptibility. The resulting H_i has been the one used for the scaling analysis. The magnetic susceptibility was measured with AC Measurement System Option in PPMS (Physical Properties Measurement System) by Quantum Design.

Single crystal neutron diffraction on a diffractometer equipped with a position sensitive detector (PSD) which covers a wide angle is a powerful tool to acquire map in reciprocal space. These maps are a very good tool to investigate magnetic structures or crystallographic superstructures from a qualitative point. Inherent to this technique is the

restriction to a 2-dimensional map when a 1-D PSD is used and the data from one map is in most cases insufficient to refine a structure model. In this experiment the cold neutron powder diffractometer DMC (Double axis MultiCounter) at the Swiss Spallation Neutron Source SINQ equipped with a 6T vertical field cryomagnet was used. The wavelength used was 2.41Å with additional pyrolytic graphite filters in the beam to suppress λ/2 contamination. The detector was set at a starting angle of 5° with the resulting coverage in $\boldsymbol{Q}$ from 0.23Å^{-1} to 3.52Å^{-1}. The Tb_3Co single crystal was oriented on a custom Al-holder in the HK0 scattering plane with the vertical magnetic field parallel to the crystallographic $\boldsymbol{c}$-direction. The crystal was then rotated around the vertical axis in 0.2° steps to cover a total of 180°. Using the software TvTueb the measured maps were transformed to HK0 reciprocal maps.

The experimental protocol was to measure maps first in zero magnetic field at 90K, 75K, 60K and 1.5K and then applying a magnetic field of 2T and measure at 1.5K, 75K and 90K.

3. Experimental results and Discussion

Fig. 1 presents the thermal diffusivity (D) of Tb_3Co as a function of temperature showing the common behavior in intermetallic materials where heat is transferred both by electrons and phonons [34, 39, 40]. From room temperature down, the electronic contribution is severely reduced due to the reduction of the resistivity while the increase in phonon contribution as the phonon mean free path increases is not enough to compensate. This general decrease stops at the magnetic phase transitions, signaled by the two dips shown in detail in the inset in Fig. 1. These dips are the common signature of magnetic phase transitions on the thermal diffusivity curves [41, 42]. After the spin ordering, the phonon mean free path greatly increases, counteracting the lesser input by electron mobility leading to a huge increase in the thermal diffusivity. It is worth noting that the curve is made up of thousands of experimental points as the temperature ramp rate is extremely low (especially in the region of the phase transitions). This allows retrieving the shape of the transitions with high resolution in order to make a quantitative treatment later on.

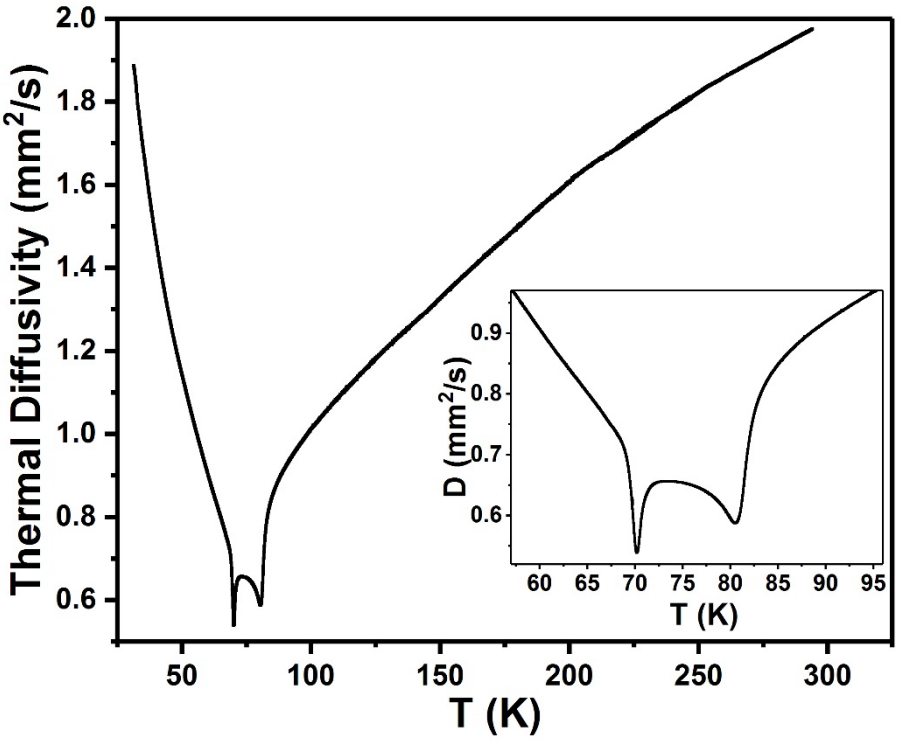

Fig. 1. Thermal diffusivity as a function of temperature for Tb_3Co showing two transitions at ≈ 70 K and ≈ 81 K. The inset shows in detail the D vs T dependence in the vicinity of the phase transitions.

It is clearly seen that there are two well separated phase transitions, the first one at 81 K, which corresponds to the PM-AFM transition, the second one at 70.2 K, with a change in magnetic ordering from AFM to FM. This attribution, in agreement with the aforementioned literature, has been corroborated by the measurement of the magnetization as a function of temperature, presented in Fig. 2.

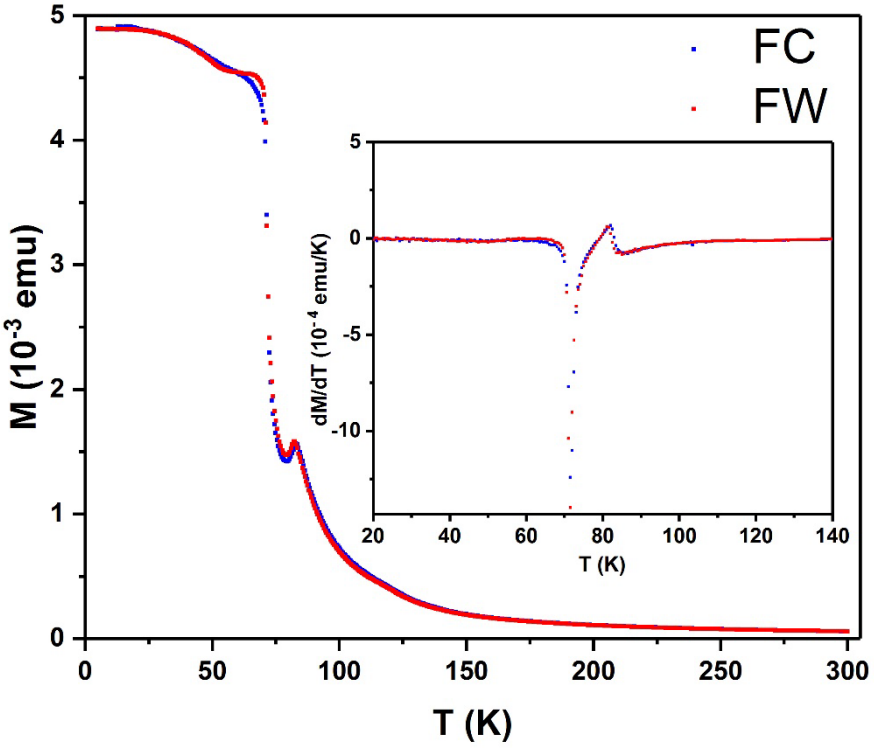

Fig. 2. Magnetization as a function of temperature for Tb_3Co, field-warmed (FW) and field-cooled (FC) measured on the plane (010) with H=100 Oe. Inset : First derivative of the magnetization.

It is commonly accepted that the PM-AFM transition is second order and our results confirm this as there is no sign of thermal hysteresis in the thermal diffusivity measurements. These measurements have been performed in heating and cooling runs with ramp rates down to 20 mK/min and neither the position nor the shape of the signal at the transition changes. This allows the use of the scaling equations from critical behavior theory to get a deeper understanding of the magnetic properties of the spins at the point of the phase transition (long or short range interactions, isotropic or anisotropic orientation of the spins) [43]. Here, both *D* and *1/D* have been fitted, using the scaling equations [44-46]

$$D = V + Wt + U^{\pm}|t|^{-b}\left(1 + F^{\pm}|t|^{0.5}\right) \quad (1)$$

$$1/D = B + Ct + A^{\pm}|t|^{-\alpha}\left(1 + E^{\pm}|t|^{0.5}\right) \quad (2)$$

where $t = (T-T_N)/T_N$ is the reduced temperature, T_N the Néel temperature, α, b are the critical exponents, while V, W, B, C, U^+, U^-, A^+, A^-, F^+, F^- E^+, E^- are adjustable parameters (the plus sign corresponds to the branches above the critical temperature, the minus sign

to the ones below it). Following renormalization group theory, the values of α, b and the ratios A^+/A^- , U^+/U^- are the ones which indicate the universality class of this transition [43-46]. The rounding of the transition, which is inherent to it and not to the technique, is not taken into account for these fittings, which are presented in Fig. 3, together with the deviation plots, which show the difference between the experimental points and the fitted curve and thus the quality of the fit. The detailed procedure to perform this kind of fitting can be found elsewhere [46].

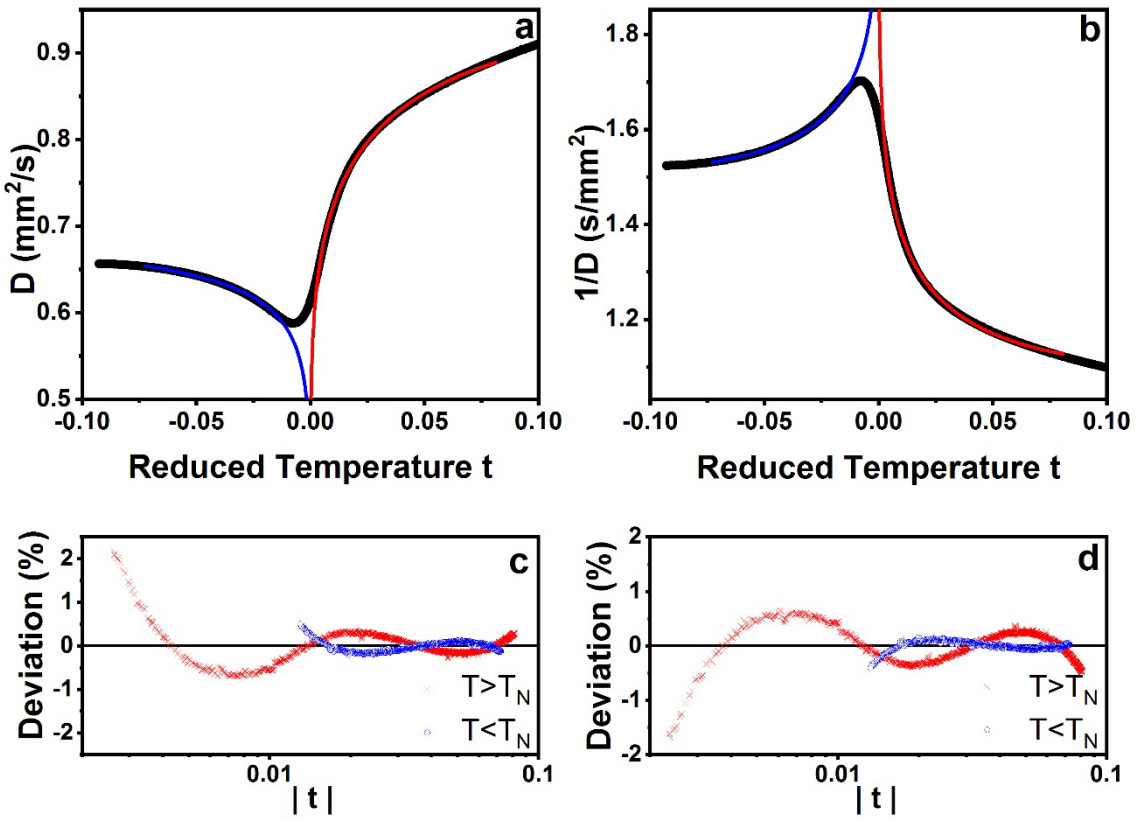

Fig. 3. a), b) Experimental thermal diffusivity and its inverse (dots) together with the fitted functions (continuous curves) to equation (1) and (2), respectively; c), d) Corresponding deviation plots: crosses for the region above the Néel temperature, circles for the region below

The fittings have given the result of α = -0.133 ± 0.008, A^+/A^- = 1.33, b = -0.136 ± 0.009, U^+/U^- = 1.2. The values of α and b agree quite well with the 3D-Heisenberg universality class (α_{theor} = -0.134 ≈ b_{theor} [46]) which implies short range order interaction of the spins and that they would have an isotropic distribution but the theoretical ratio for this model is $A^+/A^-_{\ theor}$ = 1.52 ≈ $U^+/U^-_{\ theor}$ [46]. This situation (critical exponent in agreement with the theoretical value but a smaller ratio of the critical parameters) arises when the spin distribution is not completely isotropic but without reaching the situation

in which there is an easy plane (3D-XY model, α_{theor} = -0.014) or an easy axis (3D-Ising model, α_{theor} = +0.11). Among the different mechanisms which could introduce this deviation, crystal-field effects are the most likely, due to the Tb occupancy in the orthorhombic lattice, which agrees with magnetization measurements along the principal crystallographic directions [22], where it is confirmed that, in the AFM phase, a deviation from isotropy has started to develop, which will give rise, afterwards, to the FM easy axis in the low temperature magnetic phase. Short-range order magnetic interactions at the magnetic transitions have also been proved to exist in other members of the R_3(Co;Ni) family and even surviving in the paramagnetic phase [16, 19, 47].

Regarding the AFM-FM transition at lower temperature, it is worth revising again its character, as, so far, diffraction studies have not given proof of any structural change indicating a first order phase transition, though there are several evidences of being a first order one, as explained in the Introduction.

Concerning the thermal diffusivity measurements, in order to check the possibility of a thermal hysteresis, temperature rates as low as 10 mK/min have been used in heating and cooling runs looking for a difference in the position and/or the shape of the dip, with the result shown in Fig. 4, where a slight difference is seen at 20 mK/min which is reduced at 10 mK/min, indicating that, at most, this is a weak first-order phase transition.

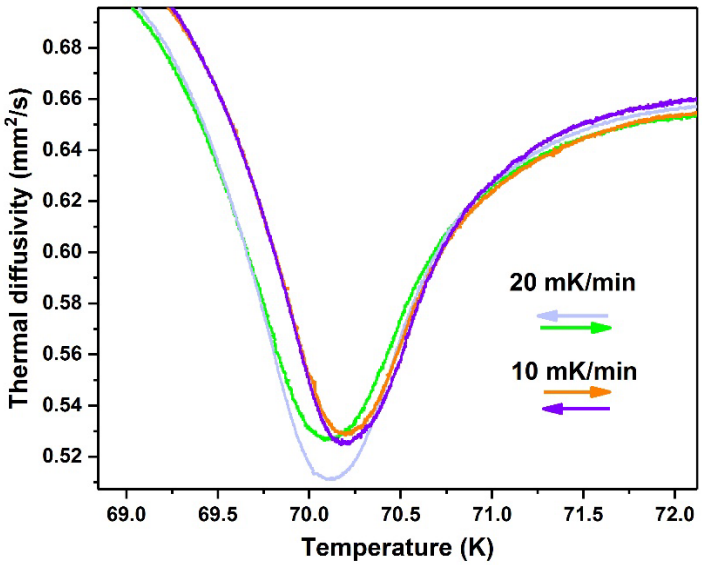

Fig. 4. Experimental thermal diffusivity curves obtained on heating and cooling at 10 mK/min and 20 mK/min to check the presence of thermal hysteresis.

Looking back to Fig. 2, no thermal hysteresis was found in the magnetization measurements on heating and cooling under an applied field (see the inset with the first derivative which marks the same position for the critical temperature), so we have looked for other ways to assess the character of this transition. In the first place, magnetization has been measured as a function of an applied magnetic field at a series of isotherms to build up the Arrott Plot (the square of the magnetization as a function of the ratio *H/M*), shown in Fig. 5, where the demagnetization factor has been taken into account, as explained in section « Samples and experimental techniques ». After the Banerjee criterion [48], if the slope of these curves is positive, the transition is second order while if it is negative it is first order. As it can be seen in the inset, at low fields the slopes are negative but only in a very short region, indicating that, indeed, the transition has a weak first order character.

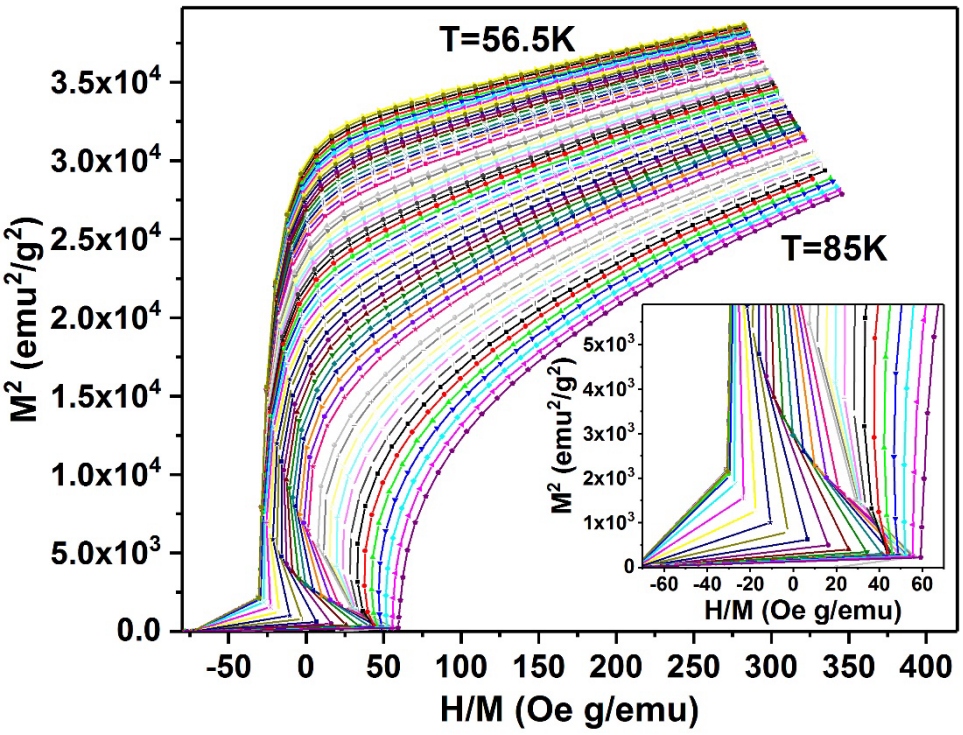

Fig 5. Arrott Plots for Tb_3Co measured on the plane (010). Inset: detail at low fields.

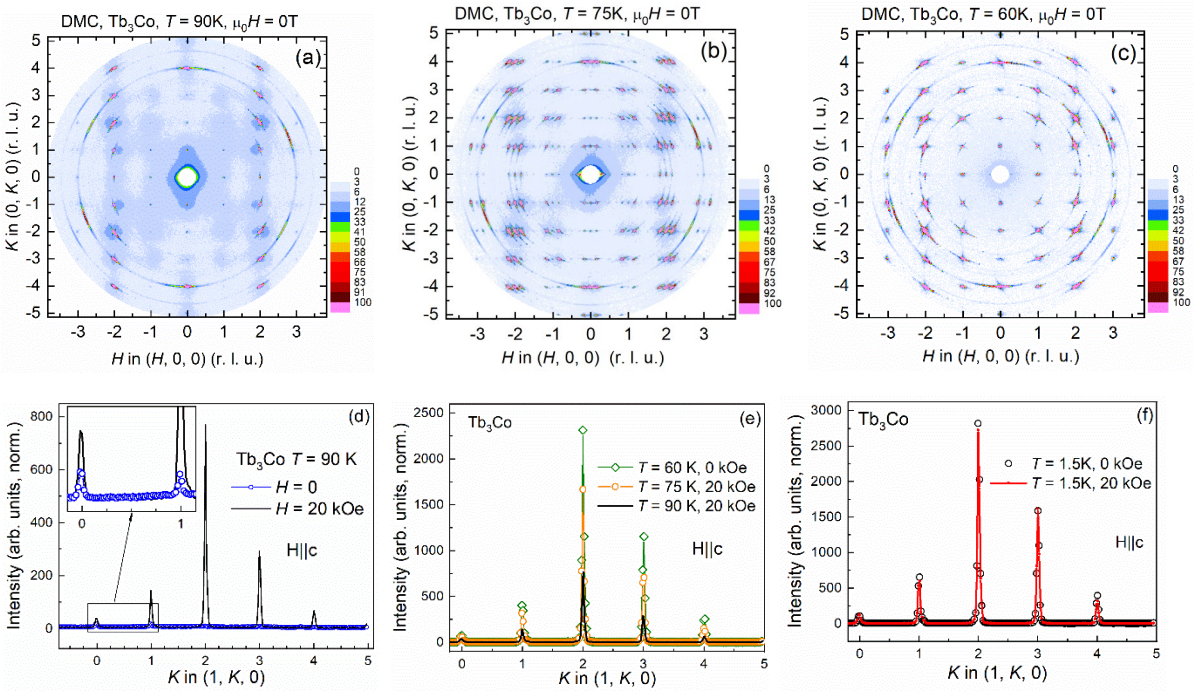

Fig. 6. Reciprocal *HK*0 map of Tb_3Co measured (a) at *T*= 90 K, (b) *T* = 75K and (c) *T* = 60 K in zero magnetic field. (d) Linecuts along 1*K*0 assessing the change of magnetic intensity in the applied magnetic field at *T* = 90K. Comparison of linecuts along 1*K*0 measured at (e) *T* = 60 K in zero magnetic field and *T* = 75 K, 90 K in the applied magnetic field and (f) at *T* = 1.5K in zero magnetic field and applied magnetic field.

Concerning the single crystal neutron diffraction measurements, Figs. 6(a)-(c) show a reciprocal *HK*0 maps of Tb_3Co measured in zero magnetic field above and below Neel temperature at *T* = 90, 75 and 60 K. The intensity is color coded and the color map has been chosen to reveal also weak intensities. In paramagnetic state at *T* = 90 K, the main structural reflections have approximately 6000 counts as peak value and if the color scale is chosen with this as maximum only the main structural peaks according to space group 62 (*Pnma*) are visible (*h*=2n, *k*=2n). This structure has been observed in a previous powder diffraction experiment [22] and the unit cell parameters estimated from our neutron diffraction data are shown in Table 1. In the chosen color scale, additional much weaker peaks (factor 100) on positions forbidden for space group 62 (*h*,*k* odd) can be found. It should be noted that a structural instability has been found in the nonmagnetic compound Y_3Co and lower symmetry space groups $P2_12_12_1$ and $P112_1$ were proposed [49]. The latter one is the highest symmetry space group which is in agreement with the observed neutron scattering pattern obtained on the Tb_3Co single crystal sample at *T* = 90 K.

Table 1. The unit cell parameters *a* and *b* of the Tb_3Co crystal structure estimated from the (200) and (040) reflection from single crystal neutron diffraction data measured in the *ab* scattering plane below and above Neel temperature T_N = 81 K in zero magnetic field and in applied magnetic field $\mu_0 H$ = 2 T. The data has been integrated along the ω-2θ line and then fitted with a Gaussian. Systematic errors from sample displacement are unaccounted for.

T (K), $\mu_0 H$ (T)	a (Å)	b (Å)
90, 0	6.886(4)	9.336(1)
75, 0	6.966(5)	9.317(1)
75, 2	6.965(1)	9.3615(5)
60, 0	6.950(1)	9.3682(5)
1.5, 0	6.931(1)	9.3186(6)
1.5, 2	6.946(1)	9.3176(7)

The magnetic scattering above T_N can be found as diffuse critical scattering around the position where magnetic Bragg peaks emerge below the ordering temperature. Interestingly the observed diffuse intensity is isotropic around the nuclear position, indicating dominating ferromagnetic correlations. However, as previously reported [22] Tb_3Co orders antiferromagnetically below T_N in an incommensurate magnetic structure with a propagation vector $\boldsymbol{k}$ = (0.155, 0, 0). The reciprocal *HK*0 map measured at T = 75 K is shown in Fig. 7b. Incommensurate magnetic satellites indexed by a propagation vector $\boldsymbol{k}$ = (0.155, 0, 0) can be seen around integer (*h*, *k*, 0)-type Bragg nodes. Below T_2 Tb_3Co becomes a ferromagnet as shown in Fig. 6(c) on the reciprocal *HK*0 map measured at T = 60 K. Intensity due to magnetic scattering is observed on all integer *HK*0 positions. The lack of a clear directional dependence indicates that the magnetic moments direction must be mainly oriented perpendicular to the scattering vector, which means the magnetic moments are mostly aligned along the crystallographic ***c***-axis. Additional reflections from a previously observed incommensurate component with the propagation vector $\boldsymbol{k}$ = (0.3, 0.3, 0) [22] cannot be seen. One possible explanation is that the cryomagnet had a small remanent magnetic field which affected the formation of the observed phase. Lowering the temperature increases the intensity due to magnetic scattering as the ordered magnetic moment follows the Brillouin function. The map at lowest temperature T = 1.5 K shows an identical pattern compared to T = 60 K.

The one-dimensional line cuts where a section is extracted from the reciprocal *HK*0 maps are shown in Figs. 6(d)-(f). The 1*K*0 linecuts for instance are a vertical line

along K on the position $H = 1$. In Fig. 6(d), two linecuts measured at 90K in zero magnetic field and in external magnetic field applied along the c crystallographic axis are plotted on top of each other. It can be seen that the ferromagnetic phase can be field induced from the paramagnetic state on application of the external magnetic along the c crystallographic axes. Fig. 6(e) compares 1K0 linecuts for different points of the ferromagnetic phase (60K, 0T; 75K, 2T and 90K, 2T). There is no change in the relative intensities between any of the observed peaks. Again, the decrease in the magnetic intensities can be explained by the reduction of the ordered magnetic moment due to thermal fluctuations. In Fig. 6(f), two linecuts are plotted on top of each other, both measured at 1.5 K. The black line comes from the measurement in zero field, the red line a vertical magnetic field of 2 T has been applied. Both linecuts are identical within the statistical error. Also, in the reciprocal maps no difference between zero and applied magnetic field can be detected. This indicates that the ferromagnetic state is indeed the ground state of Tb_3Co at below T_2. Comparing these different measurements, it can be concluded that the ferromagnetic phase found below T_2 and above a critical field are identical.

Bearing in mind magnetization data measured on the single crystal sample [23], one can conclude that application of the external magnetic field above $H_C = 5$ kOe along the c crystallographic axis results in AFM – FM type magnetic phase transition in the intermediate temperature range $T_2 < T < T_N$. This is in agreement with our neutron diffraction data measured at $T = 75$ K in external magnetic field $H = 20$ kOe. The proposed behavior of Tb_3Co in an applied magnetic field along the c-axis can be summarized with a schematic phase diagram as depicted in Fig. 7.

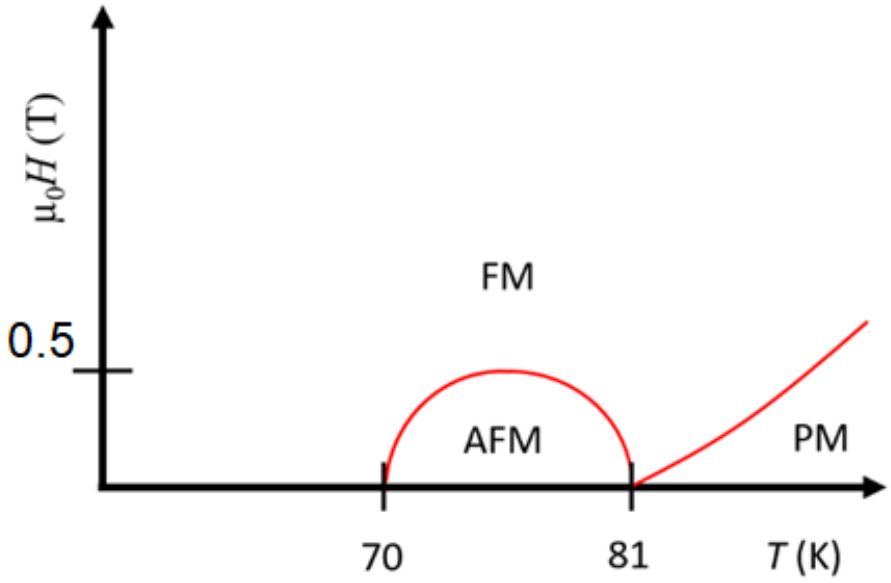

Fig. 7. Schematic phase diagram for Tb_3Co in the magnetic field applied along the *c* crystallographic direction.

The magnetocaloric properties of Tb_3Co have already been studied in literature by two groups [21, 26] using the same indirect method of evaluating the entropy change at the magnetic phase transition through the following Maxwell relation, after having measured the magnetization as a function of an applied field at a series of isotherms :

$$\Delta S_M(\mathrm{T}, \Delta \mathrm{H}) = \mu_0 \int_{H_i}^{H_f} \left(\frac{\partial M}{\partial T} \right)_H dH \qquad (3)$$

but with strong discrepancies about the values of the maximum of the magnetic entropy change as well as of the refrigerant capacity (RCP). Another very important issue is that, in both works, demagnetization effects have not been taken into account, which has been theoretically and practically demonstrated to lead to non-precise results in ΔS_M [50] or to non-universal curves [51] when the demagnetization factors are non-negligible. As there are two phase transitions and with the aim of discriminating which is responsible for the magnetocaloric effect, a detailed number of isotherms have been taken, as explained in section « Samples and experimental techniques » with the result shown in Fig. 8.

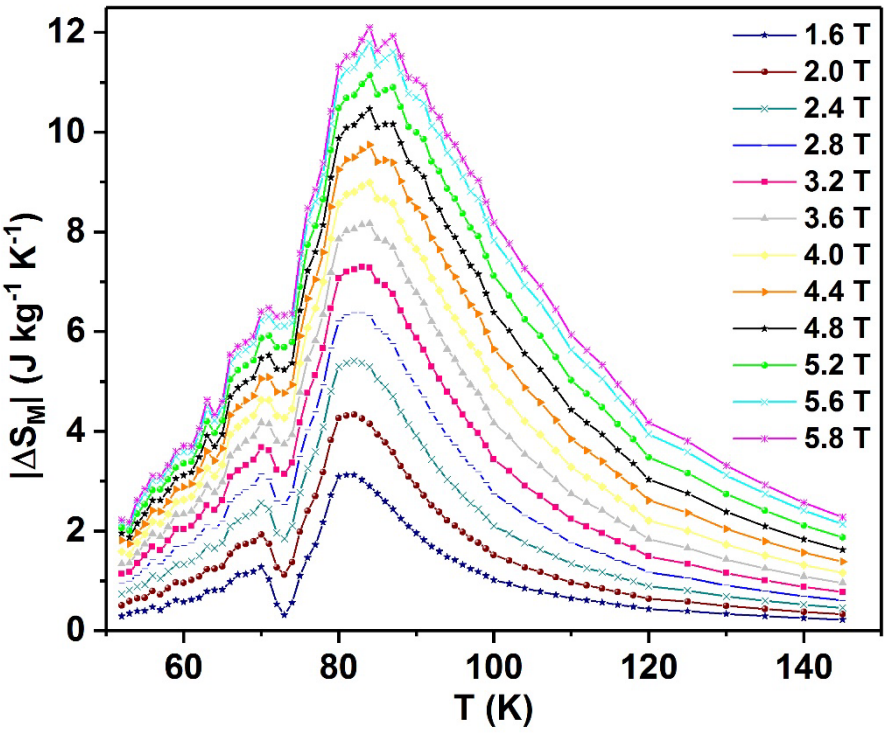

Fig. 8. Absolute value of the magnetic entropy change for Tb_3Co for different fields.

Though for small fields there is a structure in the peak of the magnetic entropy change, it is quite clear that the maximum is located at the high temperature transition and the shape of the peak is the one commonly found for second order phase transitions. It can be seen in Fig. 5 that the first order character of the low temperature transition turns into second order as the magnetic field is increased.

In order to see if, indeed, demagnetization effects are relevant, it is interesting to build up the normalized curve for the magnetic entropy change by dividing it by the corresponding maximum for the different values of the maximum applied field and rescaling the temperature axis with [52]

$$\theta = \frac{T - T_C}{T_r - T_C}, \qquad (6)$$

where T_C is the critical temperature and the reference temperature T_r is selected as that corresponding to a certain fraction of ΔS_M^{pk}, so that the curves should collapse on a master curve. Fig. 9 shows the result in this case. There, data collapse well in the vicinity of the critical temperature and above but not below the critical temperature. If increasing the applied field gives as a consequence an increase in the normalized magnetic entropy

change, the deviation is due to the presence of a demagnetization field [51, 53]; on the contrary, if the consequence is a decrease in the normalized entropy, then the physical origin of the deviation is the presence of other magnetic phases [54, 55]. The first case is of application here, which means that, indeed, the demagnetization field must be considered when calculating the peak of the magnetic entropy change or the refrigerant capacity.

Therefore, the values obtained from Fig. 8 are $\left|\Delta S_M^{pk}\right|$ = 10.73 J/kg.K and the refrigerant capacity RC_{FWHM} = 404.5 J/kg (calculated as the product of $\left|\Delta S_M^{pk}\right|$ times the width of ΔS_M at half maximum), both of them for ΔH = 5 T. The values are given at this particular field as it allows comparisons with other published results for Tb_3Co, with the consequence that they are close to those found in [26] but in clear disagreement from [21]. If we compare the values found in the current work with the ones found for other rare-earth based magnetocaloric materials in the same temperature range (se Fig. 25 in [56]) we can see that Tb_3Co is a competitive magnetocaloric material.

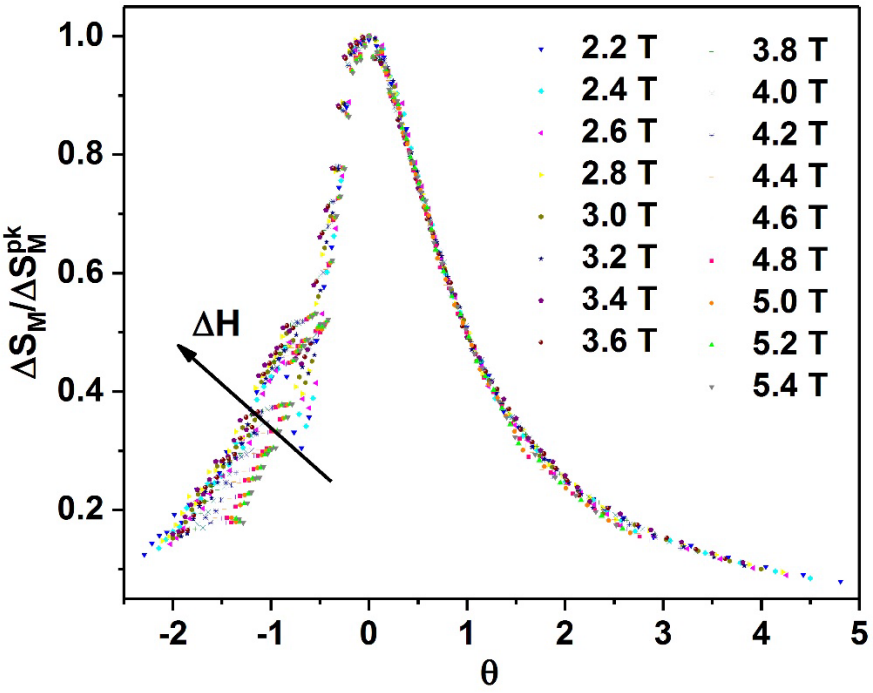

Fig. 9. Universal curve with the rescaled magnetic entropy changes for Tb_3Co using one reference temperature T_r.

Finally, the magnetocaloric effect gives us another method to check the character of the transitions, using the evolution of the exponent *n* of the field dependence of ΔS_M with temperature $n(T,H) = \frac{d\ln(\Delta S_M)}{d\ln H}$. In the case of a second order phase transition, this should tend to 1 at temperatures well below the critical one and to 2 in the paramagnetic phase, with a minimum at the Néel/Curie temperature. It has recently been proven that, if the exponent *n* shows, as a function of temperature, a peak with a maximum value well above 2, a first order phase transition is present at the position of the peak [57, 58]. Fig. 10 clearly shows that the spike indeed exists at the position of the low temperature transition, confirming its weak first order character.

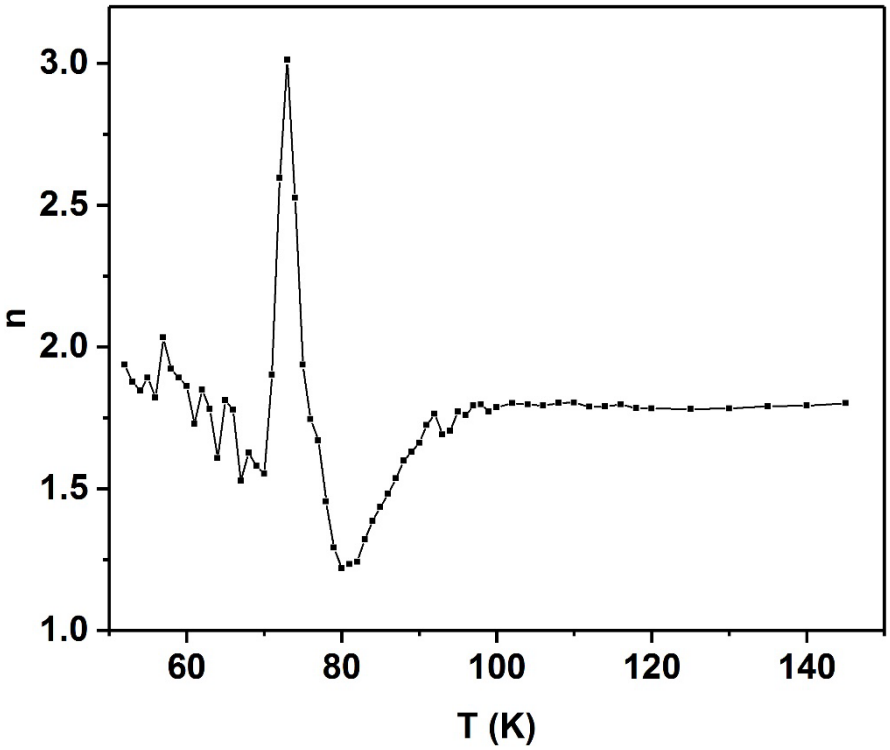

Fig 10. Dependence of the exponent *n* with temperature for ΔH= 0-2 T.

4. Conclusions

The magnetic phase transitions of Tb_3Co have been studied in detail using thermal, magnetic and neutron diffraction high resolution techniques on single crystalline samples. The PM-AFM transition which takes place at about 81 K is found to be of second order and its critical exponents are very close to the 3D-Heisenberg universality class, proving that the magnetic interactions are short-range but with a deviation from perfect isotropy

due to crystal field effects. In the AFM-FM transition at about 70 K there is no appreciable thermal hysteresis but the Arrott Plot as well as the behavior of the exponent n with temperature clearly identify it as weakly first order, giving direct evidence of its character. A weak symmetry distortion from the orthorhombic *Pnma* space group to the monoclinic symmetry consistent with the $P2_1$ space groups is found, for the first time, by the single crystal neutron diffraction in the paramagnetic state at T = 90 K. The low temperature magnetic state below T_2 was confirmed to be non-coplanar ferromagnetic structure where magnetic moments of Tb ions have strong ferromagnetic components along the crystallographic ***c***-axis. The intermediate incommensurate antiferromagnetic phase with the propagation vector $\boldsymbol{k}$ = (0.155, 0, 0) was confirmed to exist in the temperature range $T_2 < T < T_N$. The application of an external magnetic field B = 2 T along the c crystallographic axis was found to suppress the incommensurate antiferromagnetic phase and gives rise to the ferromagnetic phase. The magnetic entropy peak change as well as the refrigerant capacity, calculated taking into account demagnetization effects for a more rigorous calculation, indicate that Tb_3Co is a competitive magnetocaloric material in this temperature range.

Acknowledgements

This work has been supported by Universidad del País Vasco UPV/EHU (GIU16/93). A. Herrero thanks the Department of Education of the Basque Government as grantee of the programme "Programa Predoctoral de Formación de Personal Investigador No Doctor". The authors thank for technical and human support provided by SGIker of UPV/EHU. This material is based upon work supported by the U.S. Department of Energy, Office of Science, Office of Basic Energy Sciences, under contract number DE-AC05-00OR22725. Part of this work was performed at SINQ, Paul Scherrer Institute, Villigen, Switzerland. This work was also supported by Russian Science Foundation (project No. 18-72-10022).

REFERENCES

[1] X. Zheng, B. Shen (2017) The magnetic properties and magnetocaloric effects in binary R–T (R = Pr, Gd, Tb, Dy, Ho, Er, Tm; T = Ga, Ni, Co, Cu) intermetallic compounds, Chin. Phys. B 26:027501 (42 pp).

[2] A.M. Tishin, Y.I. Spichkin (2003) The Magnetocaloric Effect and its Applications. Series in Condensed Matter Physics, Institute of Physics Publishing, Bristol and Philadelphia.

[3] N.H. Duc, P.E. Brommer (1999) Handbook of Magnetic Materials vol 12, ed K. H. J. Buschow (Amsterdam: Elsevier Science B.V.) chapter 3 259-394.

[4] H. Kirchmayr, C.A. Poldy (1979) Handbook on Physics and Chemistry of Rare Earths vol 2, ed K. A. Gschneidner Jr and L. Eyring (Amsterdam: North-Holland) chapter 14 55-230.

[5] K.N.R. Taylor (1971) Intermetallic rare-earth compounds, Adv. Phys. 20 551-660.

[6] S.K. Tripathy, K.G. Suresh, A.K. Nigam (2006) A comparative study of the magnetocaloric effect in Gd_3Co and Gd_3Ni, J. Magn. Magn. Mat. 306:24-29.

[7] N.V. Tristan, S.A. Nikitin, T. Palewski, and K. Skokov (2002) Comparative analysis of the magnetization processes of the Gd_3Ni and Gd_3Co single crystals, J. Magn. Magn. Mat. 251:148-154.

[8] N.V. Baranov, A.V. Andreev, A.I. Kozlov, G.M. Kvashnin, H. Nakotte, H. Aruga Katori, T. Goto (1993) Magnetic phase transitions in Gd_3Co, J. Alloy. Comp. 202:215-224.

[9] N.V. Baranov, G. Hilscher, P.E Markin, H. Michor, A.A. Yermakov (2004) Spin fluctuations induced by f–d exchange in R_3T compounds, J. Magn. Magn. Mat. 272-276:637-638.

[10] N.V. Tristan, S.A. Nikitin, T. Palewski, K. Nenkov, K. Skokov (2003) Specific heat of the Gd_3Co and Gd_3Ni compounds, J. Magn. Magn. Mat. 258:583-585.

[11] N. V. Tristan, K. Nenkov, T. Palewski, K. P. Skokov, S. A. Nikitin (2003) Specific heat of the R_3Co (R = heavy rare earth or Y) compounds, Phys. Stat. Sol. (a) 196:325-328.

[12] N.V. Baranov, T. Goto, G. Hilscher, P.E. Markin, H. Michor, N.V. Mushnikov, J-G Park, A.A. Yermakov (2005) Irreversible field-induced magnetic phase transitions and properties of Ho_3Co, J. Phys.: Condens. Matter 17:3445-3462.

[13] P. Kumar, N.K. Singh, A.K. Nayak, A. Haldar, K.G. Suresh, A.K. Nigam (2010) Large reversible magnetocaloric effect in Er3Co compound, J. of App. Phys. 107:09A932 (3 pp).

[14] A.F. Gubkin, A. Podlesnyak, N.V. Baranov (2010) Single-crystal neutron diffraction study of the magnetic structure of Er_3Co, Phys. Rev. B 82:012403 (4 pp).

[15] N.V. Baranov, A.N. Pirogov, A.E. Teplykh (1995) Magnetic state of Dy_3Co, J. Alloy. Comp. 226:70-74.

[16] J. Shen, J.L. Zhao, F.X. Hu, G.H. Rao, G.Y. Liu, J.F. Wu, Y.X. Li, J. R. Sun, B. G. Shen (2010) Magnetocaloric effect in antiferromagnetic Dy_3Co compound, Appl. Phys. A 99:853-858.

[17] N.V. Baranov, E. Bauer, R. Hauser, A. Galatanu, Y. Aoki, H. Sato (2000) Field-induced phase transitions and giant magnetoresistance in Dy_3Co single crystals, Eur. Phys. J. B 16:67-72.

[18] P. Svoboda, H. Nakotte, A.M. Alsmadi, M. Doerr (2003) Magnetic Phase Diagram of Dy_3Co Single Crystal, Acta Physica Polonica B 34:1449-1452.

[19] A. Herrero, A. Oleaga, A. Salazar, A.F. Gubkin, N.V. Baranov (2018) Critical behavior of magnetic transitions in Dy_3Co single crystal, J. Alloy. Comp. 741:1163-1168.

[20] N.V. Baranov, A.V Deryagin, A.I. Kozlov, Ye.V. Sinitsyn, (1986) Field induced ferromagnetism and anomalies of the electrical resistivity in system $(Tb_{1-x}Y_x)_3Co$, Phys. Met. Metall. 61:97-106.

[21] B. Li, J. Du, W.J. Ren, W.J. Hu, Q. Zhang, D. Li, Z.D. Zhang (2008) Large reversible magnetocaloric effect in Tb_3Co compound, Appl. Phys. Lett. 92:242504 (3 pp).

[22] N.V. Baranov, A.F. Gubkin, A.P. Vokhmyanin, A.N. Pirogov, A. Podlesnyak, L. Keller, N.V. Mushnikov and M.I. Bartashevich (2007) High-field magnetization and magnetic structure of Tb_3Co J. Phys.: Condens. Matter 19:326213 (14 pp).

[23] N.V. Baranov, P.E. Markin, H. Nakotte, A. Lacerda (1998) Magnetic and transport properties of Tb_3Co studied on single crystals, J. Magn. Magn. Mat. 177-181:1133-1134.

[24] D. Gignoux, J.C. Gomez-Sal, D. Paccard (1982) Magnetic properties of a Tb_3Ni single crystal, Solid State Comm. 44: 695-700.

[25] D. Gignoux, R. Lemaire, J. Chassy (1974) Magnetic structures of the Tb_3Co compound, Proceedings of the Int. Conf. on Magnetism ICM-73, Moscow, 22-28 August 1973, vol 5, Nauka, Moscow, p. 361-363.

[26] J.C.B. Monteiro, G.A. Lombardi, R.D. doe Reis, H.E. Freitas, L.P. Cardoso, A.M. Mansanares, F.G. Gandra (2016) Heat flux measurements of Tb_3M series (M=Co, Rh and Ru): Specific heat and magnetocaloric properties, Physica B 503:64-69.

[27] U. Zammit, S. Paoloni, F. Mercuri, M. Marinelli, F. Scudieri (2012) Self consistently calibrated photopyroelectric calorimeter for the high resolution simultaneous absolute measurement of the specific heat and of the thermal conductivity, AIP Advances 2:012135 (6 pp).

[28] U. Zammit, M. Marinelli, F. Mercuri, S. Paoloni (2009) Effect of Confinement and Strain on the Specific Heat and Latent Heat over the Nematic−Isotropic Phase Transition of 8CB Liquid Crystal, J. Phys. Chem. B 113:14315-14322.

[29] U. Zammit, M. Marinelli, F. Mercuri, S. Paoloni, F. Scudieri (2011) Photopyroelectric calorimeter for the simultaneous thermal, optical, and structural characterization of samples over phase transitions, Rev. Scient. Inst. 82**:**121101 (22 pp).

[30] A. Oleaga, A. Salazar, D. Skrzypek (2015) Critical behaviour of magnetic transitions in $KCoF_3$ and $KNiF_3$ perovskites, J. Alloy. Comp. 629:178-183.

[31] A. Oleaga, V. Shvalya, V. Liubachko, G. Balakrishnan, L.D. Tung, A. Salazar (2017) Critical behavior study of the spin ordering transition in RVO3 (R = Ce, Pr, Nd, Sm, Gd, Er) by means of ac photopyroelectric calorimetry, J. Alloy. Comp. 703:210-215.

[32] M. Massot, A. Oleaga, A. Salazar, D. Prabhakaran, M. Martin, P. Berthet, G. Dhalenne (2008) Critical behavior of CoO and NiO from specific heat, thermal conductivity, and thermal diffusivity measurements, Phys. Rev. B 77:134438 (6 pp).

[33] A. Oleaga, V. Shvalya, A. Salazar, I. Stoika, Yu.M. Vysochanskii (2017) In search of a tricritical Lifshitz point in $Sn_2P_2(S_{1-x}Se_x)_6$ doped with Pb, Ge: A critical behavior study, J. Alloy. Comp. 694:808-814.

[34] A. Oleaga, V. Liubachko, P. Manfrinetti, A. Provino, Yu. Vysochanskii, A. Salazar, (2017) Critical behavior study of NdScSi, NdScGe intermetallic compounds, J. Alloy. Comp. 723:559-566.

[35] A. Herrero, A. Oleaga, P. Manfrinetti, A. Provino, A. Salazar (2018) Critical behavior of the ferromagnetic transition in GdSc(Si,Ge) intermetallic compounds, Intermetallics 101:64-71.

[36] A. Salazar (2003) On the influence of the coupling fluid in photopyroelectric measurements, Rev. Sci. Instrum. 74:825-827.

[37] W. Jiang, X.Z. Zhou, G. Williams, Y. Mukovskii, K. Glazyrin (2008) Critical behavior and transport properties of single crystal $Pr_{1-x}Ca_xMnO_3$ (x=0.27, and 0.29), Phys. Rev. B 78:144409 (10 pp).

[38] W. Jiang, X.Z. Zhou, G. Williams, Y. Mukovskii, K. Glazyrin (2008) Griffiths phase and critical behavior in single-crystal $La_{0.7}Ba_{0.3}MnO_3$: Phase diagram for $La_{1-x}Ba_xMnO_3$ ($x \leqslant 0.33$), Phys. Rev. B 77:064424 (7 pp).

[39] A.O. Oliynyk, T.D. Sparks, M.W. Gaultois, L. Ghadbeigi, A. Mar (2016) $Gd_{12}Co_{5.3}Bi$ and $Gd_{12}Co_5Bi$, Crystalline Doppelgänger with Low Thermal Conductivities, Inorganic Chem. 55:6625-6633.

[40] A.K. Bashir, M.B.T. Tchokonté, A.M. Strydom (2016) Electrical and thermal transport properties of $RECu_4Au$ compounds, RE=Nd, Gd, J. Magn. Magn. Mat. 414:69-73.

[41] A. Oleaga, A. Salazar, D. Prabhakaran, A.T. Boothroyd (2004) Critical behavior of $La_{1-x}Sr_xMnO_3$ ($0 \leqslant x \leqslant 0.35$) by thermal diffusivity measurements, Phys. Rev. B 70:184402 (7 pp).

[42] A. Oleaga, A. Salazar, H. Kuwahara (2006) Thermal diffusivity and critical behavior of $Nd_{1-x}Sr_xMnO_3$, Physica B 378-380:512-514.

[43] H.E. Stanley (1971) "Introduction to phase transitions and critical phenomena", Oxford University Press.

[44] M. Marinelli, F. Mercuri, D.P. Belanger (1995) Specific heat, thermal diffusivity, and thermal conductivity of FeF_2 at the Néel temperature, Phys. Rev. B 51:8897-8903.

[45] M. Marinelli, F. Mercuri, S. Foglietta, D.P. Belanger (1996) Effect of spin-system fluctuations on heat transport in $RbMnF_3$ close to the Néel temperature, Phys. Rev. B 54 :4087-4092.

[46] A. Salazar, M. Massot, A. Oleaga, A. Pawlak, W. Schranz (2007) Critical behavior of the thermal properties of $KMnF_3$. Phys. Rev. B 75:224428 (7 pp).

[47] N.V. Baranov, A.V. Proshkin, A.F. Gubkin, A. Cervellino, H. Michor, G. Hilscher, E.G. Gerasimov, G. Ehlers, M. Frontzek, A. Podlesnyak (2012) Enhanced survival of short-range magnetic correlations and frustrated interactions in R_3T intermetallics, J. Magn. Magn. Mat. 324:1907-1912.

[48] S.K. Banerjee (1964) On a generalised approach to first and second order magnetic transitions, Phys. Lett. 12:16-17.

[49] A. Podlesnyak, G. Ehlers, H. Cao, M. Matsuda, M. Frontzek, O. Zaharko, V. A. Kazantsev, A. F. Gubkin, N. V. Baranov (2013) Temperature-driven phase

transformation in Y_3Co: Neutron scattering and first-principles studies, Phys. Rev. B 88:024117 (7 pp).

[50] H. Neves Bez, H. Yibole, A. Pathak, Y. Mudryk, V.K. Pecharsky (2018) Best practices in evaluation of the magnetocaloric effect from bulk magnetization measurements, J. Magn. Magn. Mat. 458:301-309.

[51] R. Caballero-Flores, V. Franco, A. Conde, L.F. Kiss (2009) Influence of the demagnetizing field on the determination of the magnetocaloric effect from magnetization curves, J. Appl. Phys. 105:07A919 (3 pp).

[52] V. Franco, A. Conde, J.M. Romero-Enrique, J.S. Blázquez (2008) A universal curve for the magnetocaloric effect: ananalysis based on scaling relations, J. Phys.: Condens. Matter 20:285207 (5pp).

[53] S. Couillaud, E. Gaudin, V. Franco, A. Conde, R. Pöttgen, B. Heying, U.Ch. Rodewald, B. Chevalier (2011) The magnetocaloric properties of GdScSi and GdScGe, Intermetallics 19:1573-1578.

[54] V. Franco, R. Caballero-Flores, A. Conde, Q.Y. Dong, H.W. Zhang (2009) The influence of a minority magnetic phase on the field dependence of the magnetocaloric effect J. Magn. Magn. Mat. 321 :1115-1120.

[55] V. Franco, A. Conde, V. Provenzano, R.D. Shull (2010) Scaling analysis of the magnetocaloric effect in $Gd_5Si_2Ge_{1.9}X_{0.1}$ (X=Al, Cu, Ga, Mn, Fe, Co), J. Magn. Magn. Mat. 322:218-223.

[56] V. Franco, J.S. Blázquez, J.J. Ipus, J.Y. Law, L.M. Moreno-Ramírez, A. Conde (2018) Magnetocaloric effect: From materials research to refrigeration devices, Progress in Materials Science 93:112–232.

[57] J.Y. Law, V. Franco, L.M. Moreno-Ramírez, A. Conde, D.Y. Karpenkov, I. Radulov, K.P. Skokov, O. Gutfleisch (2018) A quantitative criterion for determining the order of magnetic phase transitions using the magnetocaloric effect, Nat. Comm. 9:2680 (8 pp).

[58] L.M. Moreno-Ramírez, C. Romero-Muñiz, J.Y. Law, V. Franco, A. Conde, I. Radulov, F. Maccari, K.P. Skokov, O. Gutfleisch (2018) The role of Ni in modifying the order of the phase transition of $La(Fe,Ni,Si)_{13}$, Acta Materialia 160:137-146.

FIGURE CAPTIONS

Fig. 1. Thermal diffusivity as a function of temperature for Tb_3Co showing two transitions at ≈ 70 K and ≈ 81 K. The inset shows in detail the D vs T dependence in the vicinity of the phase transitions.

Fig. 2. Magnetization as a function of temperature for Tb_3Co, field-warmed (FW) and field-cooled (FC) measured on the plane (010) with H=100 Oe. Inset : First derivative of the magnetization.

Fig. 3. a), b) Experimental thermal diffusivity and its inverse (dots) together with the fitted functions (continuous curves) to equation (1) and (2), respectively; c), d) Corresponding deviation plots: crosses for the region above the Néel temperature, circles for the region below

Fig. 4. Experimental thermal diffusivity curves obtained on heating and cooling at 10 mK/min and 20 mK/min to check the presence of thermal hysteresis.

Fig 5. Arrott Plots for Tb_3Co measured on the plane (010). Inset: detail at low fields.

Fig. 6. Reciprocal $HK0$ map of Tb_3Co measured (a) at T= 90 K, (b) T = 75K and (c) T = 60 K in zero magnetic field. (d) Linecuts along $1K0$ assessing the change of magnetic intensity in the applied magnetic field at T = 90K. Comparison of linecuts along $1K0$ measured at (e) T = 60 K in zero magnetic field and T = 75 K, 90 K in the applied magnetic field and (f) at T = 1.5K in zero magnetic field and applied magnetic field.

Figure 7. Schematic phase diagram for Tb_3Co in the magnetic field applied along the c crystallographic direction.

Fig. 8. Absolute value of the magnetic entropy change for Tb_3Co for different fields.

Fig. 9. Universal curve with the rescaled magnetic entropy changes for Tb_3Co using one reference temperature T_r.

Fig 10. Dependence of the exponent *n* with temperature for ΔH= 0-2 T.